Developmental Biology 370 (2012) 154–163

Contents lists available at SciVerse ScienceDirect

Developmental Biology

journal homepage: www.elsevier.com/locate/developmentalbiology

Muscle contraction controls skeletal morphogenesis through regulation of chondrocyte convergent extension

Yulia Shwartz [a], Zsuzsanna Farkas [b], Tomer Stern [a], Attila Aszódi [b], Elazar Zelzer [a,*]

[a] Department of Molecular Genetics, Weizmann Institute of Science, PO Box 26, Rehovot 76100, Israel
[b] Department of Surgery, Ludwig-Maximilians University, Munich, Germany

ARTICLE INFO

Article history:
Received 9 May 2012
Received in revised form
23 July 2012
Accepted 25 July 2012
Available online 2 August 2012

Keywords:
Chondrocyte intercalation
Convergent extension
Muscle contraction
Mechanical load
Paralysis
Skeletogenesis
Pharyngeal cartilage
Zebrafish

ABSTRACT

Convergent extension driven by mediolateral intercalation of chondrocytes is a key process that contributes to skeletal growth and morphogenesis. While progress has been made in deciphering the molecular mechanism that underlies this process, the involvement of mechanical load exerted by muscle contraction in its regulation has not been studied. Using the zebrafish as a model system, we found abnormal pharyngeal cartilage morphology in both chemically and genetically paralyzed embryos, demonstrating the importance of muscle contraction for zebrafish skeletal development. The shortening of skeletal elements was accompanied by prominent changes in cell morphology and organization. While in control the cells were elongated, chondrocytes in paralyzed zebrafish were smaller and exhibited a more rounded shape, confirmed by a reduction in their length-to-width ratio. The typical columnar organization of cells was affected too, as chondrocytes in various skeletal elements exhibited abnormal stacking patterns, indicating aberrant intercalation. Finally, we demonstrate impaired chondrocyte intercalation in growth plates of muscle-less Sp^{d} mouse embryos, implying the evolutionary conservation of muscle force regulation of this essential morphogenetic process.Our findings provide a new perspective on the regulatory interaction between muscle contraction and skeletal morphogenesis by uncovering the role of muscle-induced mechanical loads in regulating chondrocyte intercalation in two different vertebrate models.

Introduction

Muscle contraction has long been known to regulate skeletogenesis. Analyses of chemically paralyzed chick embryos and mutant mouse embryos that lacked muscle contraction have revealed its involvement in various aspects of skeletogenesis, such as joint development (Kahn et al., 2009; Nowlan et al., 2010; Pai, 1965; Pitsillides, 2006; Tremblay et al., 1998), bone ridge development (Blitz et al., 2009; Hall and Herring, 1990; Hamburger, 1940; Hosseini and Hogg, 1991; Pai, 1965; Rot-Nikcevic et al., 2006; Tremblay et al., 1998) and bone morphogenesis (Nowlan et al., 2008; Sharir et al., 2011). In humans, restricted fetal movement may lead to fetal akinesia deformation sequence syndrome (FADS [OMIM 208150]), a condition characterized by a variety of deformities, including skeletal abnormalities.

Although the contribution of muscle contraction to skeletogenesis has become evident, the underlying cellular and molecular mechanisms are still largely missing. The transparency of the zebrafish embryo allows for fine resolution cellular analysis. Moreover, the ease of genetic manipulations in this species facilitates the deciphering of molecular pathways. These features make the zebrafish an attractive model system for studying the involvement of muscle contraction in skeletal development.

In recent years, the genetic and morphological aspects of zebrafish craniofacial development have been extensively studied (Kimmel et al., 2001; Knight and Schilling, 2006; Piotrowski et al., 1996; Schilling, 1997; Schilling et al., 1996; Yelick and Schilling, 2002). Similarly to long bones of higher vertebrates, craniofacial bones of zebrafish develop by a process termed endochondral ossification. During this process, mesenchymal cells condense and differentiate to chondrocytes, which proliferate to form a cartilaginous anlage that is later replaced by bone (Provot and Schipani, 2005). During endochondral ossification, the mediolateral intercalation of chondrocytes into columns is an important module that facilitates elongation and contributes to bone morphology (Ahrens et al., 2009; Aszodi et al., 2003; Bengtsson et al., 2005; Clement et al., 2008; Dodds, 1930; Gao et al., 2011; Keller et al., 2000; Kimmel et al., 1998; LeClair et al., 2009; Li and Dudley, 2009; Sarmah et al., 2010; Yang et al., 2003). Cell intercalation is a morphogenetic process, which occurs in epithelial or mesenchymal cells and leads to tissue narrowing, known as convergence, and its elongation, or extension. During convergent extension, the

* Corresponding author.
E-mail address: eli.zelzer@weizmann.ac.il (E. Zelzer).

0012-1606/$ - see front matter © 2012 Elsevier Inc. All rights reserved.
http://dx.doi.org/10.1016/j.ydbio.2012.07.026

intercalating cell moves to separate neighboring cells, while staying in the same plane. During intercalation, cells increase their length-to-width ratio, perpendicularly to the direction of tissue elongation (Davidson et al., 2010). In recent years, several molecules have been implicated in regulating chondrocyte intercalation (Ahrens et al., 2009; Aszodi et al., 2003; Bengtsson et al., 2005; Clement et al., 2008; Gao et al., 2011; LeClair et al., 2009; Li and Dudley, 2009; Sarmah et al., 2010; Yang et al., 2003); However, an involvement of mechanical load in this process has not been reported yet.

In this study, we demonstrate the pivotal role of muscle contraction in chondrocyte intercalation by analyzing paralyzed zebrafish. Moreover, we show the evolutionary conservation of this effect in mice.

Materials and methods

Animals

Fish were bred and raised under standard conditions. *nic* mutants (b107) were generated by crossing heterozygous parents (Walker and Streisinger, 1983; Westerfield et al., 1990). *sox*10-GFP transgenic zebrafish were described previously (Carney et al., 2006; Wada et al., 2005). Morpholino antisense oligonucleotides against *myf*5 and *myod* were described previously (Hinits et al., 2009). Heterozygous Sp^{d} mice were previously described (Dickie, 1964).

Tricaine immobilization

Zebrafish were immobilized by 0.016% tricaine in fish water containing methylene blue (sigma MB1); the solution was changed every 2 days (Westerfield, 2000).

Skeletal preparations

For visualization of pharyngeal cartilage elements, flat mount preparations were made by microdissection as previously described (Javidan and Schilling, 2004). Alcian blue (Sigma) staining was performed as previously described (Javidan and Schilling, 2004) with minor modifications to the clearing process. Tissues were first cleared in 0.05% trypsin, then subjected to additional clearing in 1.8% KOH, washed and gradually transferred to 70% glycerol.

Histology and in situ hybridization

Mouse embryos were fixed in 4% paraformaldehyde (PFA) at 4 °C overnight. Fixed samples were embedded in paraffin and sectioned at 7-μm thickness. Hematoxylin and eosin (H&E) staining was performed following standard protocols. Cell morphology was assessed using rhodamine-conjugated phalloidin (Sigma) to visualize filamentous actin. Alternatively, mouse embryos were fixed in 4% PFA for 6–8 h at room temperature, and then transferred into 30% sucrose at 4 °C overnight. The samples were embedded in O.C.T. compound and 50 μm frozen sections were cut using a cryostat.

Zebrafish whole-mount in situ hybridization was performed as previously described (Thisse and Thisse, 2008). Antisense probes were generated using the following primers: *barx*1: forward, cgagcgtcagtcaaaagttctcca, reverse, aggagacaccggaaacttcaggat; *sox*9*a*: forward, aaaagcgagcaccgtggatttg, reverse, gacgcttttccacctcgttcagta; *col2a*1: forward, gcaaagggacagaaaggagaacca, reverse, caccatcacttccgggttttcca.

Immunohistochemistry

For zebrafish whole-mount staining, embryos were fixed in 4% PFA and dehydrated in methanol. Then, zebrafish were rehydrated in PBS and permeabilized with proteinase K. The primary antibody against type II collagen (II-II6B3; Developmental Studies Hybridoma Bank, The University of Iowa) was diluted 1:100, followed by a secondary antibody staining using Cy3 anti-mouse (Jackson) diluted 1:100. 4',6-diamidino-2-phenylindole (DAPI) was used for counterstaining.

Cell number quantification

In zebrafish, cells were counted manually in col2a1- and DAPI-stained preparations photographed by an LSM 510 confocal microscope. To capture the entire skeletal element, *Z* stacks were used. In mice, cells occupying a constant area of 8732.73 μm^2 were counted manually in phalloidin- and DAPI-stained preparations.

Zebrafish phenotype variation

Both *nic* mutants and *myf*5/*myod* double morphants exhibited a variety of phenotypes, mostly of chondrocyte stacking patterns. The phenotypes ranged from almost normal stacking to a severely malformed pattern, which is described in the 'Results' section. *sox*9*a* in situ hybridization of 72 hpf *nic* mutants also showed variation; the abnormal expression pattern is described in the 'Results' section.

Cell morphology analysis

In mice, images of phalloidin stained paraffin or O.C.T. sections were used. In zebrafish, images of *col2a*1 and Alcian blue staining were used for morphological analysis. To characterize chondrocyte elongation, the long and short axes of the cells were measured to calculate length-to-width ratio.

Growth plate length measurements

Phalloidin-stained paraffin sections were used to measure the length of the growth plate, defined as the distance from the epiphysis to the end of the hypertrophic chondrocytes.

Column analysis

For column length and angle analysis, phalloidin-stained paraffin sections were used. For length assessment, individual columns were manually identified and the cells composing the column were counted.

For angle analysis, each column was represented by a line segment bisecting the column along its longitudinal axis and defined by its start and end points. All segments were marked manually on each of the analyzed images. The calculation was restricted to pairs of columns with a potential for intercalation, based on the following criteria: 1. The minimal distance between the two segments is not more than a predefined length; 2. A normal line extending from one segment intersects the other segment.

For each pair of segments that meet the criteria, the smaller angle between them was calculated, resulting in an angle within the range [0°,90°]. Then, for each image all angles were grouped into bins of 5°, to form a single histogram.

Statistical methods

All variables are presented as mean ± standard deviation from the mean (SD). Statistical significance was determined as a p-value of 0.05 or less. For analysis of ceratohyal length and angle, the ratio between stacked to unstacked length and cell number in the ceratohyal cartilage in zebrafish, a two-tailed Student's t-test was used. The same test was used for assessment of growth plate length and number of cells per area in mice. To analyze column length, a Poisson regression was used. The number of cells in a column was the dependent variable and the genotype was the independent variable. For cell morphology analysis (length-to-width ratio) both in mice and zebrafish, a linear mixed model (LMM) was used on the log ratio. The LMM approach was used to incorporate the variance between embryos in mice and zebrafish and the variance between sections in the embryo in mice.

For column angle analysis, we used a modification of the logistic decay model, as follows:

$$y = f(angle) = Asym\left(1 - \frac{1}{1+\exp((xmid - angle)/scal)}\right)$$

where *Asym* is the initial *Y*-axis value, meaning the prevalence of parallel columns (0–5° angle), *xmid* is the angle at which the value of *Y* equals *Asym*/2, and *scal* affects the decay rate and is also used for scaling. The model was fitted for each genotype for both humerus and femur in the framework of nonlinear mixed effects models, in order to incorporate the random differences between embryos within the same genotype. Initial results showed that there were no significant differences in the *scal* parameter between the genotypes, both in the humerus ($z = -0.80439$, $p = 0.4226$) and femur ($z = -0.0744$, $p = 0.9408$). Thus, we refitted the model such that the *scal* parameter was common for both genotypes within each growth plate.

Results

Muscle contraction is essential for proper pharyngeal cartilage morphogenesis

In zebrafish, pharyngeal cartilage develops early during development in a time window that enables the survival of paralyzed embryos, since at that stage there is no active feeding. To determine the role of muscle contraction in pharyngeal cartilage formation, movement, hence load application, was prevented by anesthetizing embryos with tricaine at 8.5 h post fertilization (hpf; 75% epiboly stage), prior to somitogenesis (Kimmel et al., 1995). Embryos were then allowed to develop under paralysis until 120 hpf and viability was confirmed by the presence of a heartbeat.

When compared to the control, paralyzed embryos exhibited reduced jaw and head size, pericardial edema and unabsorbed yolk sac (Fig. 1A). Alcian blue staining was reduced, revealing a significant reduction in the size of all pharyngeal cartilage elements in paralyzed zebrafish, compared to control embryos (Fig. 1A, D). In addition, there was a marked enlargement of the angle between skeletal elements and the midline in the paralyzed larvae (Fig. 1A, E). Interestingly, this difference was already apparent at 72 hpf (Supplementary Fig. S1).

To demonstrate the specificity of the paralysis effect on the forming skeleton, we examined two additional genetically paralyzed models: *nic* mutant and *myf5/myod* double morphant (MO). *nic* mutants are paralyzed due to a mutation in the nicotinic receptor, which prevents accumulation of functional nicotinic receptors at the neuromuscular junction (Walker and Streisinger, 1983; Westerfield et al., 1990), whereas *myf5/myod* MO exhibits complete absence of head musculature (Chen and Tsai, 2002; Hinits et al., 2009, 2011;Lin et al., 2006). With minor variations, the phenotypes of *nic* mutants and *myf5/myod* MO strongly resembled that of tricaine-treated embryos (Fig. 1B–E). Furthermore, Alcian blue staining revealed a change in relative location between Meckel's and ceratohyal cartilages and between Meckel's cartilage and the neurocranium in both models (Fig. 1B, C). These changes were visible in bright field images of all three models (Fig. 1A–C).

These results imply that muscle contraction is essential for normal craniofacial development in the zebrafish embryo.

In the absence of muscle contraction neural crest cells migrate and differentiate

Zebrafish pharyngeal cartilage is derived from cranial neural crest cells that migrate to populate seven pharyngeal arches, which serve as a common primordium for various skeletal elements (Knight and Schilling, 2006; Schilling and Kimmel, 1994). To test whether impaired neural crest specification and migration contributes to the pharyngeal cartilage phenotype in the absence of muscle contraction, we analyzed *sox*10-GFP transgenic zebrafish, in which both premigratory and migratory neural crest cells are labeled (Carney et al., 2006; Wada et al., 2005). At 25 hpf, there was no significant difference in either level or pattern of *sox*10 expression between paralyzed and control embryos (Fig. 2A). This result indicates that differences in specification and migration of neural crest cells cannot account for the skeletal aberrations observed in the absence of muscle contraction.

A reduction in Alcian blue staining (Fig. 1) may indicate a delay in chondrocyte differentiation or reduced glycosaminoglycan production. To test whether muscle contraction plays a role in cartilage differentiation, we analyzed expression of several chondrogenic markers in both *nic* mutants and tricaine-paralyzed embryos. We performed whole-mount in situ hybridization for *sox*9*a*, a zebrafish co-ortholog that is essential for chondrocyte differentiation and cartilage formation (Yan et al., 2002, 2005), for *col2a*1, which encodes the major cartilage matrix protein type II collagen (Bell et al., 1997) and for *barx*1, which is important for the proliferation of arch progenitors, chondrocyte condensation and differentiation (Sperber and Dawid, 2008; Tissier-Seta et al., 1995). At 48 hpf in both control and paralyzed zebrafish, *sox*9*a* was expressed in the first two pharyngeal arches and in the neurocranium, whereas *col2a*1 was expressed only in the neurocranium. At that stage, *barx*1 was expressed in all seven pharyngeal arches both in control and in paralyzed embryos (Fig. 2Ba and Supplementary Fig. S2Aa). Later, at 72 hpf, *sox*9*a*, *col2a*1 and *barx*1 were detected both in control and paralyzed embryos in Meckel's cartilage, palatoquadrate, ceratohyal cartilage and in the ceratobranchials. However, there were marked differences in the expression levels, as *sox*9*a* and *col2a*1 expressions were reduced in the ceratobranchials and *sox*9*a* expression was elevated in the ceratohyal and Meckel's cartilage in paralyzed embryos compared to control embryos (Fig. 2Bb and Supplementary Fig. S2Ab).

To assess the completion of chondrocyte differentiation, we performed *col2a*1 immunostaining in control and paralyzed (*nic* and tricaine-treated) zebrafish at 120 hpf. In all three groups, all pharyngeal cartilage elements were stained, although the paralyzed zebrafish exhibited abnormal morphology as described above (Fig. 2C and Supplementary Fig. S2B).

Next, to assess whether reduced cell number contributes to aberrant skeletal morphogenesis, we compared the number of cells composing the ceratohyal cartilage between control embryos and *nic* mutants. Surprisingly, chondrocyte count did not reveal any significant differences (Fig. 2D), suggesting that another mechanism must

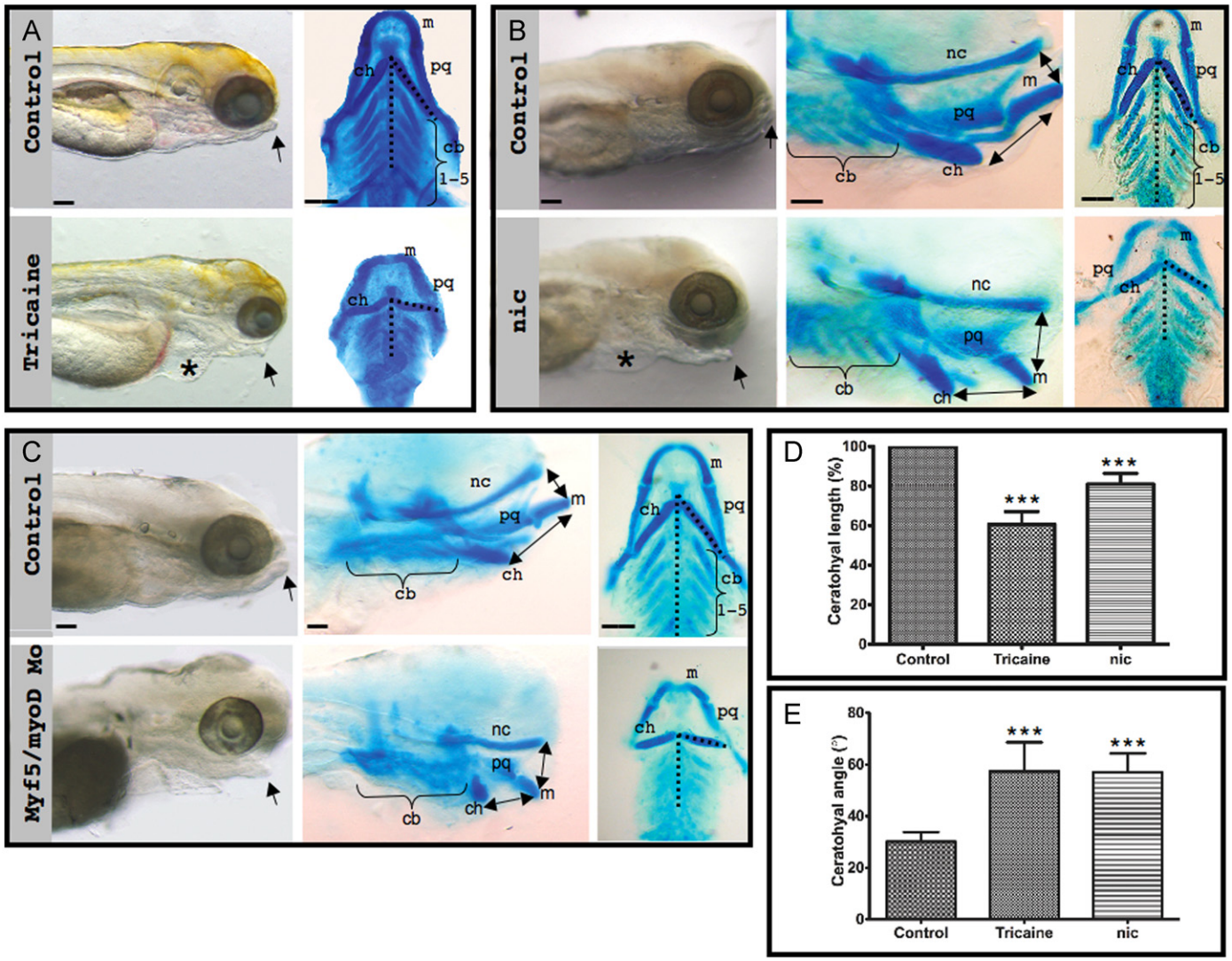

Fig. 1. Muscle contraction is necessary for craniofacial morphogenesis. (A) Left: Lateral view of control and tricaine-paralyzed zebrafish embryos at 120 hpf, using bright field microscopy. Right: Ventral view of flat-mounted Alcian blue stained control and tricaine-paralyzed zebrafish. (B) Left: Lateral view using bright field microscopy of control and *nic* mutant 120 hpf embryos. Lateral view (middle) and flat-mounted ventral view (right) of control and *nic* mutant zebrafish stained with Alcian blue. (C) Left: Lateral view using bright field microscopy of control and *myf5/myod* double morphant zebrafish at 120 hpf. Lateral view (middle) and flat-mounted ventral view (right) of control and *myf5/myod* embryos stained with Alcian blue. Asterisk indicates pericardial edema (A, B). Arrows indicate lower jaw (A)–(C). Double-headed arrows indicate relative location between Meckel's and ceratohyal cartilages and between Meckel's cartilage and the neurocranium (B, C). (D) Graph showing the reduction in ceratohyal length in paralyzed zebrafish compared to control ($p < 0.0001$). Both right and left ceratohyal cartilages from twelve tricaine-paralyzed, eight *nic* mutant and a corresponding number of control embryos were measured at 120 hpf. (E) Graph showing the increase in the angle between ceratohyal cartilage and the midline (dashed line in A–C) in tricaine-paralyzed and *nic* mutant embryos compared to control ($p < 0.0001$). The angle of both right and left ceratohyal cartilage of 6 tricaine-paralyzed and 11 *nic* mutants at 120 hpf was measured. Scale bars represent 100 μm. Abbreviations: m: Meckel's cartilage, ch: ceratohyal cartilage, cb: ceratobranchials, pq: palatoquadrate, nc: neurocranium.

account for the skeletal abnormalities observed in the absence of muscle contraction.

Muscle contraction is necessary for convergent extension in cartilage

Convergent extension movements, including chondrocyte elongation and intercalation along the mediolateral axis of the tissue, are essential for proper morphogenesis of bones that develop via cartilaginous intermediates. To visualize cellular organization within the pharyngeal cartilage, we performed Alcian blue staining of both control and *nic* zebrafish at 120 hpf. The skeletal elements of control embryos comprised flat, elongated cells, whose long axes were perpendicular to the elongation axis of the element, creating a typical stacking pattern (Fig. 3A, Ba–c). In contrast, various skeletal elements of the *nic* mutant exhibited abnormal pattern of chondrocyte stacking, characterized by increased cell-to-neighbors contacts compared to the control (Fig. 3A). To further explore the effect of muscle contraction on cell intercalation, we examined chondrocyte morphology in tricaine-paralyzed and *myf5/myod* double morphants. Analysis of the ceratohyal cartilage showed that chondrocytes in all the models were smaller and exhibited a less elongated morphology; this finding was confirmed by a significant reduction in the mean length-to-width ratio in both *nic* and tricaine paralyzed embryos (Fig. 3Ba–d). Taken together, the observed changes in cell organization and morphology indicate aberrant intercalation in the absence of muscle contraction.

Since all the phenotypes described above were the consequence of long-term paralysis, it was possible that they were caused by an indirect effect. Therefore, to test the direct involvement of muscle contraction in chondrocyte intercalation, embryos were allowed to develop normally until 96 hpf and were then paralyzed for 24 h. We hypothesized that a direct involvement

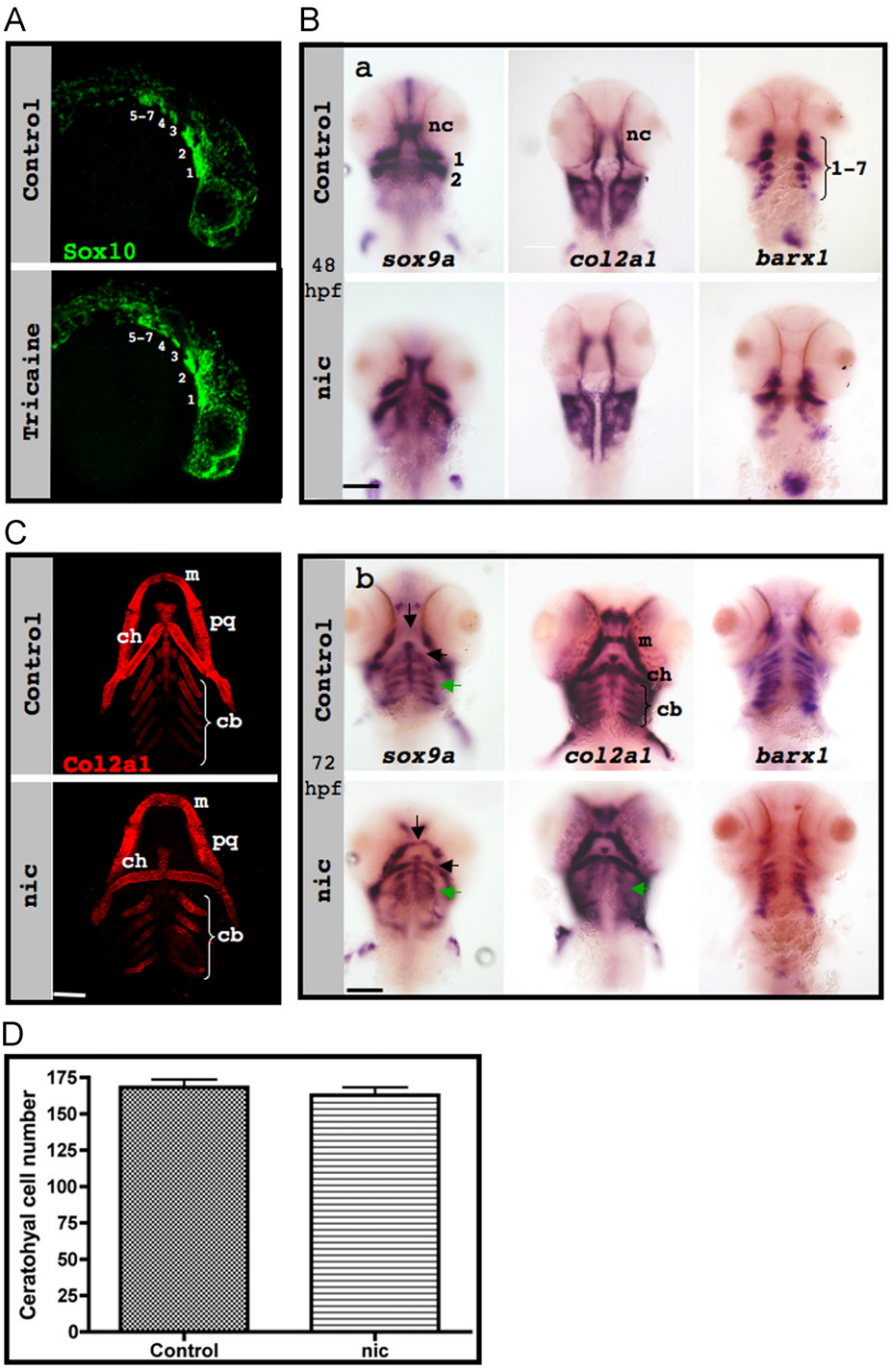

Fig. 2. Neural crest specification, migration and differentiation in the absence of muscle contraction. (A) *sox*10 expression (green) in confocal images of control (upper panel) and paralyzed (lower panel) 25 hpf zebrafish embryos; numbers indicate pharyngeal arches. (B) In situ hybridization of control (upper panels) and *nic* mutant (lower panels) embryos demonstrates the expression patterns of *sox*9*a* (left), *col*2*a*1 (middle) and *barx*1 (right) at 48 hpf (a) and at 72 hpf (b). Green arrows indicate ceratobranchial cartilage, and black arrows indicate Meckel's cartilage and ceratohyal cartilage. (C) Immunostaining for *col*2*a*1 (red) of control (upper panel) and *nic* mutant 120 hpf zebrafish (lower panel). (D) Counting of cells that compose both ceratohyal cartilages of five controls and six 120 hpf *nic* mutants ($p=0.4909$). Scale bars are 100 μm.

would lead to an increase in the number of unstacked cells in response to paralysis (Fig. 4A). Examination of ceratohyal cartilage in paralyzed embryos showed an increase in the length of the area occupied by unstacked chondrocytes, compared to control embryos (Fig. 4B). This observation was quantitatively verified by a significant increase in the ratio of the lengths of the areas of unstacked to stacked chondrocytes in paralyzed embryos, compared to control (Fig. 4C). Together, these changes in chondrocyte morphology and organization imply that muscle contraction is a major regulator of chondrocyte intercalation in zebrafish, thereby contributing to the elongation of skeletal elements.

Muscle contraction involvement in column formation is evolutionarily conserved

Our finding that muscle contractions regulate chondrocyte intercalation in zebrafish raised an interesting question regarding the conservation across species of this effect. To address this

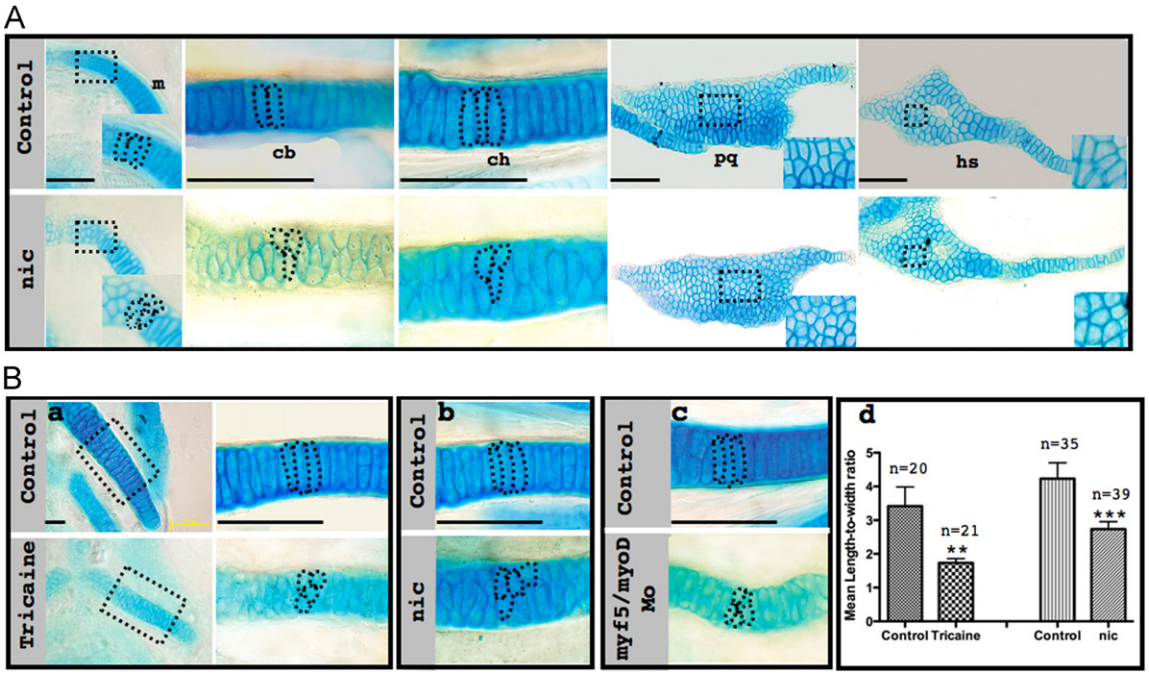

Fig. 3. Muscle contraction is essential for creating proper stacking pattern. (A) Flat-mounted Alcian blue stained control (upper panel) and *nic* mutant (lower panel) 120 hpf zebrafish show the difference in cell morphology in various skeletal elements. Magnifications of squared areas are shown in the lower right corner. Dashed lines demarcate individual cells. (B) Flat-mounted Alcian blue stained control (upper panel) and tricaine-paralyzed (lower panel) ceratohyal cartilage at 120 hpf (a). Right: Magnification of squared areas; dashed lines demarcate individual cells. Flat-mounted Alcian blue stained ceratohyal cartilage from a corresponding location as shown in (a) from control embryos (upper panels), *nic* mutant (b, lower panel) and *myf*5/*myod* double morphants (c, lower panel) at 120 hpf. Quantification of length-to-width ratio (d) in cells from the middle part of the ceratohyal cartilage of control, tricaine-paralyzed ($F_{13.887}=35.63$, $p=0.004$) and *nic* mutant ($F_{1,72}=55.44$, $p=1.65E\text{-}10$) embryos; *n* represents number of measured cells; scale bars represent 50 μm.

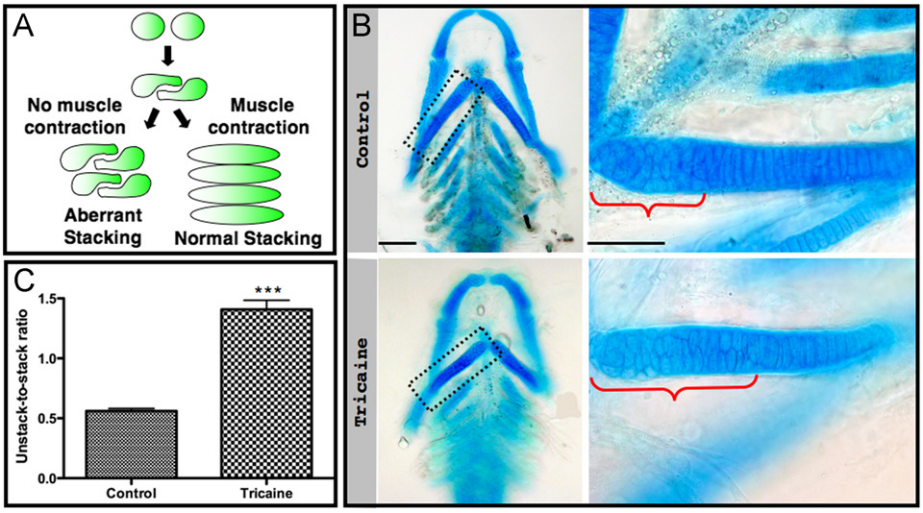

Fig. 4. Short-term paralysis results in aberrant stacking. (A) A model illustrating the involvement of muscle contraction in chondrocyte intercalation (modified from Li and Dudley, 2009). (B) Flat-mounted Alcian blue stained control (upper panel) and tricaine-paralyzed (lower panel) 120 hpf zebrafish. Magnifications of the boxed areas are shown on the right. Brackets indicate the length of the area occupied by unstacked chondrocytes. Scale bars are 100 μm on the left and 50 μm on the right. (C) Quantification of the ratio of the lengths of areas of unstacked to stacked chondrocytes in four controls and four paralyzed zebrafish ($p<0.0001$).

question, we analyzed a murine model devoid of limb musculature named splotch delayed (Sp^d), in which a point mutation in the *Pax*3 gene leads to a defect in migration of muscle progenitor cells to the developing limb (Franz, 1993; Tremblay et al., 1998). We examined bone elongation at two locations: the proximal growth plate of the humerus and the distal growth plate of the femur. Our analysis revealed a significant reduction of approximately 10% in the length of both growth plates (Fig. 5A), which could not be attributed to a decrease in cell number (Fig. 5B).

The two main mechanisms of proximodistal growth plate elongation are oriented cell division and mediolateral chondrocyte intercalation. During mammalian growth plate development, mediolaterally elongated chondrocytes in the proliferative zone divide orthogonally to this axis. Then, the semicircular daughter cells intercalate back via different wedge-shape stages, until they achieve their flattened shape in the same longitudinally oriented stack. The formation of extended columns may depend on two sequential morphogenetic processes: first the intercalation movements between

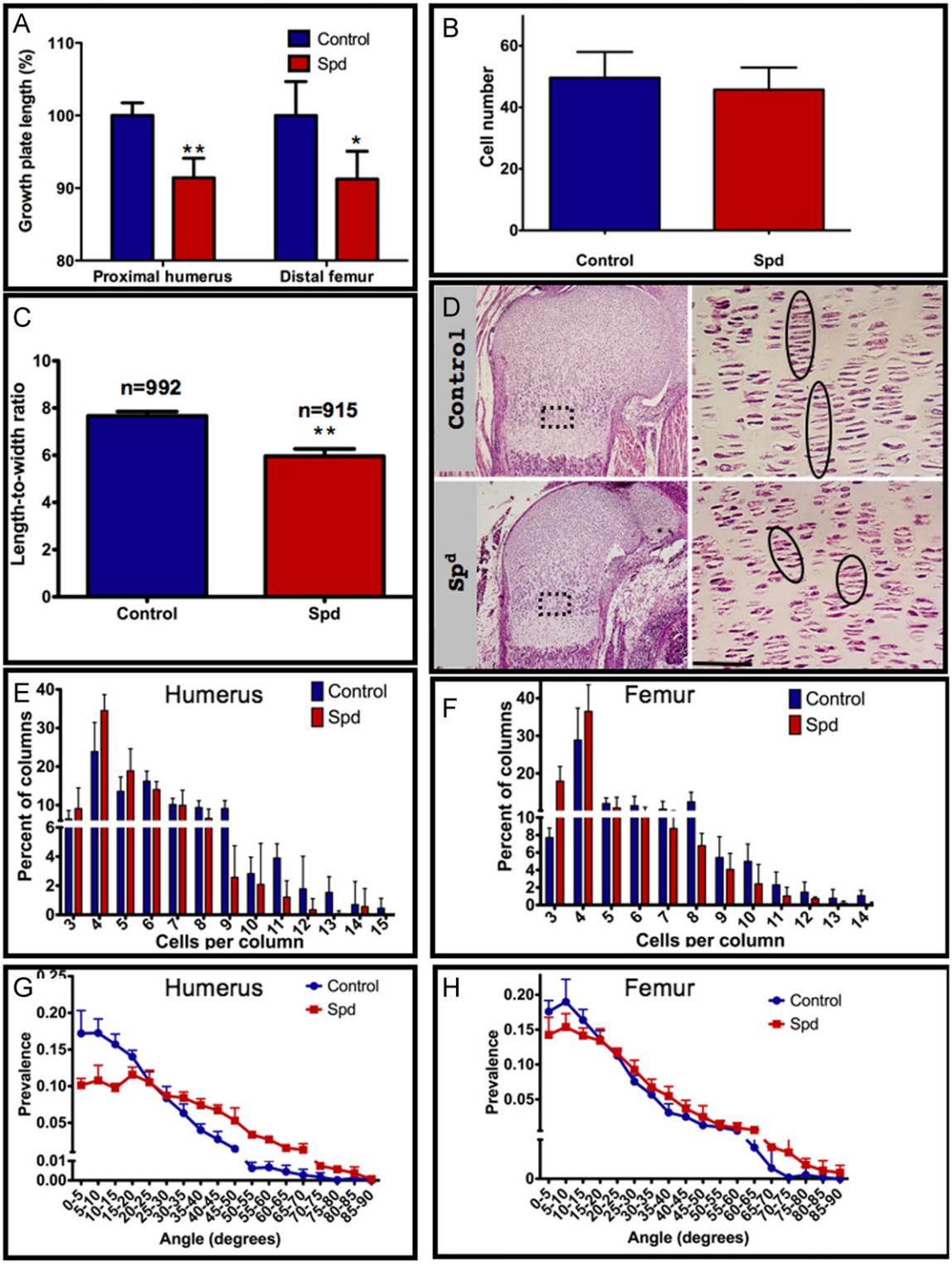

Fig. 5. Muscle contraction affects chondrocyte intercalation in mice. (A) Length measurements of humeral and femoral growth plates in control and Sp^d mutant (humerus: $p=0.0017$; femur: $p=0.027$). (B) Quantification of cell number per constant area in control and Sp^d embryos ($p=0.1266$). An area of 8732.73 μm^2, corresponding to the boxed area in (D) in the humerus growth plate was used for calculation; 4–7 sections from each embryo were analyzed. (C) Quantification of the mean length-to-width ratio of chondrocytes from control and Sp^d humeral growth plates ($F_{15,5}=71.07$, $p=0.0002$). (D) H&E staining of control (upper panel) and Sp^d (lower panel) humeral growth plates; magnification of the boxed areas is shown on the right. Circles highlight the columnar organization of chondrocytes. (E, F) Comparison of chondrocyte column lengths between control and Sp^d embryos: Distribution of columns by number of cells per column in the humerus (E; $X_1^2=13.093$, $p=0.0003$) and femur (F; $X_1^2=14.192$, $p=0.00017$). (G, H) Distribution of angles between adjacent columns in control and Sp^d mutant in the humerus (G) and femur (H). Both distributions were found to be significantly different (see Tables 1 and 2). Measurements were made on 4–5 controls and 4–5 mutant embryos from 3–4 different litters; scale bar represents 50 μm.

individual postmitotic cells within the stack, followed by merging of shorter stacks into a continuous longitudinal column (Johnstone et al., 2000b). To quantify the change in chondrocyte geometry from semicircular into longer and thinner cells, we measured length-to-width ratio of proliferating chondrocytes in controls and Sp^d mutants humerus growth plate at embryonic day 18.5 (E18.5). We observed a

Table 1
Nonlinear mixed effect model for the humerus. Analysis of the angles between chondrocyte columns in the humerus, using a modification of the logistic decay model. For a detailed description of parameters and model application, see the 'Materials and Methods' section.

	Value	Std. error	DF	*Z*	*p*-value
Asym Sp^d	0.108	0.0027	132	40.2681	
xmid Sp^d	44.052	1.04429	132	42.18441	
scal Sp^d	9.551	0.6874	132	13.8956	
Asym WT–Asym Sp^d	0.086	0.0066	132	12.99314	> 1e-10
xmid WT–xmid Sp^d	−21.478	1.3221	132	−16.24451	> 1e-10

Table 2
Nonlinear mixed effect model for the femur. Analysis of the angles between chondrocyte columns in the femur, using a modification of the logistic decay model. For a detailed description of parameters and model application, see the 'Materials and Methods' section.

	Value	Std. error	DF	*Z*	*p*-value
Asym. Sp^d	0.1566	0.008	132	19.3638	
xmid. Sp^d	29.418	1.6675	132	17.6417	
scal. Sp^d	8.4975	0.7705	132	11.0279	
Asym. wt–Asym. Sp^d	0.043	0.0118	132	3.63279	0.0004
xmid. wt–xmid. Sp^d	−7.375	2.354	132	−3.1319	0.0021

significant 30% reduction in the mean ratio in Sp^d mutants, compared to control cells (Fig. 5C). Despite the significant change in cell shape, columns still formed in the absence of muscle contraction; however, histologically, the columns in the Sp^d mutant growth plate appeared shorter, suggesting that either the postmitotic intercalation or the stack merging process was less efficient. To validate the histological observation, we compared cell number in columns of control and Sp^d mutant growth plates. As can be seen in Fig. 5D, proliferating chondrocytes in Sp^d growth plate intercalated into shorter columns, compared to the control. To quantify this difference, we compared the distribution of columns by cell number in both the humeral and femoral growth plates between control and mutant embryos. Our analysis revealed a significant difference in the column length distribution between control and Sp^d mutants. Sp^d growth plates exhibited a higher percent of short columns and lower percent of long columns than the control (Fig. 5E, F).

Little is known on the mechanism that guides two short columns to intercalate into one long column (Johnstone et al., 2000b). We hypothesized that in order for two columns to undergo successful intercalation, they need to be co-aligned such that chondrocytes can slide on each other. We further postulated that muscle contraction may be necessary for the alignment of short columns and that the failure in column intercalation in its absence could be caused by misalignment. To test this hypothesis, we measured the angle between adjacent columns in humeral and femoral growth plates of control and Sp^d mutants. Our analysis demonstrated that in the mutant growth plates, the columns were significantly more oblique-angled than in the control (Fig. 5G, H and Tables 1 and 2).

Together, these results suggest that in mice, muscle load is involved in extended column formation by regulating short column orientation. This implies cross-species conservation of muscle contraction-dependent regulation of chondrocyte intercalation.

Discussion

Intercalation is a morphogenetic process during which epithelial or mesenchymal cells move to separate neighboring cells, while staying in the same plane. Previous studies demonstrate that chondrocyte intercalation is a central process in bone elongation, which is conserved from basal vertebrates such as lampreys (Martin et al., 2009) to mammals. In mammalians, postmitotic chondrocytes in the developing growth plate undergo mediolateral intercalation, leading to the formation of the stereotypical columnar structure that drives longitudinal bone growth (Ahrens et al., 2009; Aszodi et al., 2003; Dodds, 1930; Gao et al., 2011; Li and Dudley, 2009; Yang et al., 2003). Chondrocyte intercalation was also shown to be important for zebrafish craniofacial development, by promoting elongation of skeletal elements (Clement et al., 2008; Kimmel et al., 1998; LeClair et al., 2009; Piotrowski et al., 1996; Sarmah et al., 2010).

The molecular mechanism that regulates column formation via chondrocyte intercalation has only recently begun to be uncovered. Several molecules, including members of Wnt-PCP pathway, cell–matrix adhesion molecules such as integrins and various matrix components were reported to contribute to this process (Ahrens et al., 2009; Aszodi et al., 2003; Bengtsson et al., 2005; Clement et al., 2008; Gao et al., 2011; LeClair et al., 2009; Li and Dudley, 2009; Sarmah et al., 2010; Yang et al., 2003).

Here, we firmly establish muscle load as a major player in regulating chondrocyte intercalation. The significance of this finding lies in the fact that a tight coordination must exist during embryogenesis between the forming skeleton and musculature to ensure proper development, assembly and function of the musculoskeleton system. Regulation of chondrocyte intercalation and skeletal elongation by muscle contraction facilitates such coordination. A logical extension of this notion is the expected cross-species conservation of this mechanism. Interestingly, recent studies in drosophila link mechanical signals to cell polarization, which is a prerequisite for proper intercalation (Aigouy et al., 2010; Olguin et al., 2011).

Indeed, our finding that in growth plates of muscle-less mice, chondrocyte intercalation is affected demonstrates the importance of this mechanism. Nevertheless, unlike the severe effect on intercalation observed in zebrafish, in mice the effect was only partial. While the variation between zebrafish and mouse phenotypes is an open question, it may be attributed to differences in complexity and size between the species. In the zebrafish, skeletal structures are formed by basic intercalation of a relatively small number of cells. Conversely, the elongation and shaping of long bones of a mouse may involve sequential steps of intercalation, first between postmitotic cells and then between columns. Our finding that in mice, unlike in zebrafish, columns are formed in the absence of muscle contraction indicates that the first step of intercalation is mostly muscle independent. However, we show that in mice, muscle contraction controls the second process of column intercalation, most likely through regulation of the alignment of shorter chondrocyte stacks (Fig. 6). This suggests that in the course of evolution, although the involvement of muscle contraction in the regulation of chondrocyte intercalation has been conserved, the mode of involvement has changed. Once the mechanism that integrates mechanical signals into molecular machinery is identified, it may be possible to further elucidate these differences between species.

While aberrant chondrocyte intercalation is responsible for the shortening of skeletal elements in paralyzed zebrafish and mice, the reason for enlargement of the angle between ceratohyal cartilage and the midline in paralyzed zebrafish larvae remains elusive. In the normal course of development, ceratohyal angle is reduced. Concurrently, the head muscles develop and start to function while skeletal elements undergo significant elongation (Schilling and Kimmel, 1997); these processes do not occur in paralyzed zebrafish. Given this, a plausible explanation for ceratohyal angle enlargement is reduction in the posterior pull that acts on cartilage anlagen. Alternatively, it may be the consequence of cartilage growth inhibition, as under normal conditions rapid growth in length may lead to angle reduction.

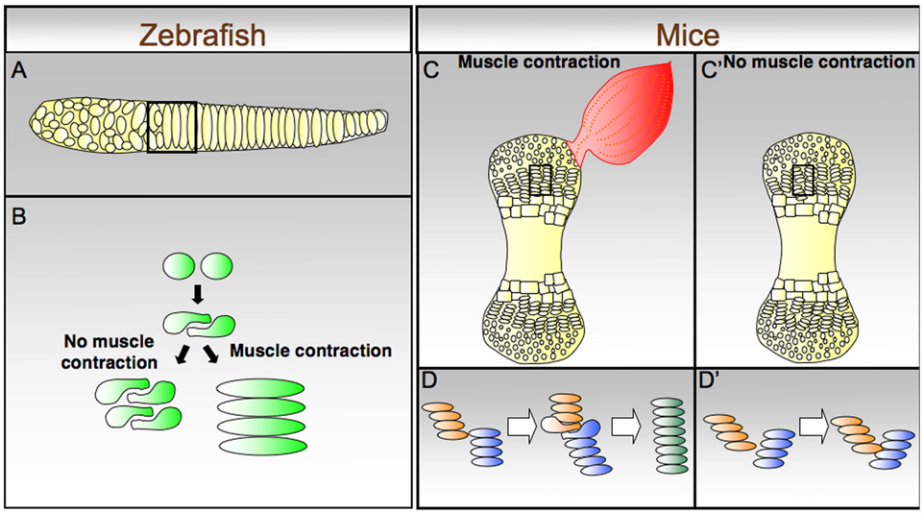

Fig. 6. Muscle involvement in chondrocyte intercalation in zebrafish and mice. (A, B) A model illustrating the involvement of muscle contraction in chondrocyte intercalation in the zebrafish embryo. The ceratohyal cartilage, schematically represented in (A), is formed by chondrocyte intercalation. The contribution of muscle contraction is vital for the creation of a normal stacking pattern (B). (C–D') A model illustrating the involvement of muscle contraction in chondrocyte intercalation in the mouse embryo. Schematic representation of the cartilaginous template of a long bone exposed to (C) and devoid of (C') muscle contraction. (D, D'): A magnification of the boxed areas in (C, C') shows that muscle contraction is crucial for correct alignment of adjacent columns, which is required for their intercalation and for the resulting growth plate elongation.

In conclusion, our study demonstrates the centrality of muscle contraction in zebrafish skeletogenesis. On a cellular level, our findings link mechanical load and chondrocyte intercalation, a process crucial for morphogenesis of skeletal elements. This establishes muscle contraction as a key regulator of skeletal structure and function.

Acknowledgments

We thank N. Konstantin for expert editorial assistance, S. Krief for expert technical support and all members of the Zelzer laboratory for advice and suggestions. We thank Dr. Y. Parmet from the Weizmann Institute of science for his statistical analysis expertise. We are grateful to Dr. K. Yaniv from the Department of Biological Regulation at the Weizmann Institute of Science and all members of the Yaniv Laboratory for advice and assistance in all aspects of work with the zebrafish model. We are grateful to Prof. T.F. Schilling for providing us with the Sox10-GFP line.

This work was supported by grants from the Israel Science Foundation (ISF, Grants 1206/09), Minerva Foundation (Grant M1138), The Y. Leon Benoziyo Institute for Molecular Medicine, Helen and Martin Kimmel Institute for Stem Cell Research, J&R Center for Scientific Research, Estate of Raymond Lapon, Estate of David Levinson, The Leo and Julia Forchheimer Center for Molecular Genetics, and Marla L. Schaefer, New York, NY, USA. E.Z. is the incumbent of the Martha S. Sagon Career Development Chair.

Appendix A. Supporting information

Supplementary data associated with this article can be found in the online version at http://dx.doi.org/10.1016/j.ydbio.2012.07.026.

References

Ahrens, M.J., Li, Y., Jiang, H., Dudley, A.T., 2009. Convergent extension movements in growth plate chondrocytes require gpi-anchored cell surface proteins. Development 136, 3463–3474.

Aigouy, B., Farhadifar, R., Staple, D.B., Sagner, A., Roper, J.C., Julicher, F., Eaton, S., 2010. Cell flow reorients the axis of planar polarity in the wing epithelium of Drosophila. Cell 142, 773–786.

Aszodi, A., Hunziker, E.B., Brakebusch, C., Fassler, R., 2003. Beta1 integrins regulate chondrocyte rotation, G1 progression, and cytokinesis. Genes Dev. 17, 2465–2479.

Bell, D.M., Leung, K.K., Wheatley, S.C., Ng, L.J., Zhou, S., Ling, K.W., Sham, M.H., Koopman, P., Tam, P.P., Cheah, K.S., 1997. Sox9 directly regulates the type-II collagen gene. Nat. Genet. 16, 174–178.

Bengtsson, T., Aszodi, A., Nicolae, C., Hunziker, E.B., Lundgren-Akerlund, E., Fassler, R., 2005. Loss of alpha10beta1 integrin expression leads to moderate dysfunction of growth plate chondrocytes. J. Cell Sci. 118, 929–936.

Blitz, E., Viukov, S., Sharir, A., Shwartz, Y., Galloway, J.L., Pryce, B.A., Johnson, R.L., Tabin, C.J., Schweitzer, R., Zelzer, E., 2009. Bone ridge patterning during musculoskeletal assembly is mediated through SCX regulation of Bmp4 at the tendon–skeleton junction. Dev. Cell 17, 861–873.

Carney, T.J., Dutton, K.A., Greenhill, E., Delfino-Machin, M., Dufourcq, P., Blader, P., Kelsh, R.N., 2006. A direct role for Sox10 in specification of neural crest-derived sensory neurons. Development 133, 4619–4630.

Chen, Y.H., Tsai, H.J., 2002. Treatment with Myf5-morpholino results in somite patterning and brain formation defects in zebrafish. Differentiation 70, 447–456.

Clement, A., Wiweger, M., von der Hardt, S., Rusch, M.A., Selleck, S.B., Chien, C.B., Roehl, H.H., 2008. Regulation of zebrafish skeletogenesis by ext2/dackel and papst1/pinscher. PLoS Genet. 4, e1000136.

Davidson, L.A., Joshi, S.D., Kim, H.Y., von Dassow, M., Zhang, L., Zhou, J., 2010. Emergent morphogenesis: elastic mechanics of a self-deforming tissue. J. Biomech. 43, 63–70.

Dickie, M.M., 1964. New Splotch Alleles in the Mouse. J. Hered. 55, 97–101.

Dodds, G.S., 1930. Row formation and other types of arrangement of cartilage cells in endochondral ossification. Anat. Rec. 46, 385–399.

Franz, T., 1993. The Splotch (Sp1H) and Splotch-delayed (Spd) alleles: differential phenotypic effects on neural crest and limb musculature. Anat. Embryol. (Berlin) 187, 371–377.

Gao, B., Song, H., Bishop, K., Elliot, G., Garrett, L., English, M.A., Andre, P., Robinson, J., Sood, R., Minami, Y., Economides, A.N., Yang, Y., 2011. Wnt signaling gradients establish planar cell polarity by inducing Vangl2 phosphorylation through Ror2. Dev. Cell 20, 163–176.

Hall, B.K., Herring, S.W., 1990. Paralysis and growth of the musculoskeletal system in the embryonic chick. J. Morphol. 206, 45–56.

Hamburger, V.a., W., M., 1940. The primary development of the skeleton in nerveless and poorly innervated limb transplants of chick embryos. Physiol. Zool. 13, 367–384.

Hinits, Y., Osborn, D.P., Hughes, S.M., 2009. Differential requirements for myogenic regulatory factors distinguish medial and lateral somitic, cranial and fin muscle fibre populations. Development 136, 403–414.

Hinits, Y., Williams, V.C., Sweetman, D., Donn, T.M., Ma, T.P., Moens, C.B., Hughes, S.M., 2011. Defective cranial skeletal development, larval lethality and haploinsufficiency in Myod mutant zebrafish. Dev. Biol. 358, 102–112.

Hosseini, A., Hogg, D.A., 1991. The effects of paralysis on skeletal development in the chick embryo I. General effects. J. Anat. 177, 159–168.

Javidan, Y., Schilling, T.F., 2004. Development of cartilage and bone. Methods Cell Biol. 76, 415–436.

Johnstone, E.W., Leane, P.B., Kolesik, P., Byers, S., Foster, B.K., 2000b. Spatial arrangement of physeal cartilage chondrocytes and the structure of the primary spongiosa. J. Orthop. Sci. 5, 294–301.
Kahn, J., Shwartz, Y., Blitz, E., Krief, S., Sharir, A., Breitel, D.A., Rattenbach, R., Relaix, F., Maire, P., Rountree, R.B., Kingsley, D.M., Zelzer, E., 2009. Muscle contraction is necessary to maintain joint progenitor cell fate. Dev. Cell 16, 734–743.
Keller, R., Davidson, L., Edlund, A., Elul, T., Ezin, M., Shook, D., Skoglund, P., 2000. Mechanisms of convergence and extension by cell intercalation. Philos. Trans. R. Soc. London B Biol. Sci. 355, 897–922.
Kimmel, C.B., Ballard, W.W., Kimmel, S.R., Ullmann, B., Schilling, T.F., 1995. Stages of embryonic development of the zebrafish. Dev. Dyn. 203, 253–310.
Kimmel, C.B., Miller, C.T., Kruze, G., Ullmann, B., BreMiller, R.A., Larison, K.D., Snyder, H.C., 1998. The shaping of pharyngeal cartilages during early development of the zebrafish. Dev. Biol. 203, 245–263.
Kimmel, C.B., Miller, C.T., Moens, C.B., 2001. Specification and morphogenesis of the zebrafish larval head skeleton. Dev. Biol. 233, 239–257.
Knight, R.D., Schilling, T.F., 2006. Cranial neural crest and development of the head skeleton. Adv. Exp. Med. Biol. 589, 120–133.
LeClair, E.E., Mui, S.R., Huang, A., Topczewska, J.M., Topczewski, J., 2009. Craniofacial skeletal defects of adult zebrafish Glypican 4 (knypek) mutants. Dev. Dyn. 238, 2550–2563.
Li, Y., Dudley, A.T., 2009. Noncanonical frizzled signaling regulates cell polarity of growth plate chondrocytes. Development 136, 1083–1092.
Lin, C.Y., Yung, R.F., Lee, H.C., Chen, W.T., Chen, Y.H., Tsai, H.J., 2006. Myogenic regulatory factors Myf5 and Myod function distinctly during craniofacial myogenesis of zebrafish. Dev. Biol. 299, 594–608.
Martin, W.M., Bumm, L.A., McCauley, D.W., 2009. Development of the viscerocranial skeleton during embryogenesis of the sea lamprey, petromyzon marinus. Dev. Dyn. 238, 3126–3138.
Nowlan, N.C., Murphy, P., Prendergast, P.J., 2008. A dynamic pattern of mechanical stimulation promotes ossification in avian embryonic long bones. J. Biomech. 41, 249–258.
Nowlan, N.C., Sharpe, J., Roddy, K.A., Prendergast, P.J., Murphy, P., 2010. Mechanobiology of embryonic skeletal development: insights from animal models. Birth Defects Res. C Embryo Today. 90, 203–13.
Olguin, P., Glavic, A., Mlodzik, M., 2011. Intertissue mechanical stress affects frizzled-mediated planar cell polarity in the Drosophila notum epidermis. Curr. Biol. 21, 236–242.
Pai, A.C., 1965. Developmental genetics of a lethal mutation, muscular dysgenesis (Mdg), in the mouse. I. Genetic analysis and gross morphology. Dev. Biol. 11, 82–92.
Piotrowski, T., Schilling, T.F., Brand, M., Jiang, Y.J., Heisenberg, C.P., Beuchle, D., Grandel, H., van Eeden, F.J., Furutani-Seiki, M., Granato, M., Haffter, P., Hammerschmidt, M., Kane, D.A., Kelsh, R.N., Mullins, M.C., Odenthal, J., Warga, R.M., Nusslein-Volhard, C., 1996. Jaw and branchial arch mutants in zebrafish II: anterior arches and cartilage differentiation. Development 123, 345–356.
Pitsillides, A.A., 2006. Early effects of embryonic movement: 'a shot out of the dark'. J. Anat. 208, 417–431.
Provot, S., Schipani, E., 2005. Molecular mechanisms of endochondral bone development. Biochem. Biophys. Res. Commun. 328, 658–665.
Rot-Nikcevic, I., Reddy, T., Downing, K.J., Belliveau, A.C., Hallgrimsson, B., Hall, B.K., Kablar, B., 2006. Myf5-/-:MyoD-/- amyogenic fetuses reveal the importance of early contraction and static loading by striated muscle in mouse skeletogenesis. Dev. Genes Evol. 216, 1–9.
Sarmah, S., Barrallo-Gimeno, A., Melville, D.B., Topczewski, J., Solnica-Krezel, L., Knapik, E.W., 2010. Sec24D-dependent transport of extracellular matrix proteins is required for zebrafish skeletal morphogenesis. PLoS One 5, e10367.
Schilling, T.F., 1997. Genetic analysis of craniofacial development in the vertebrate embryo. BioEssays 19, 459–468.
Schilling, T.F., Kimmel, C.B., 1994. Segment and cell type lineage restrictions during pharyngeal arch development in the zebrafish embryo. Development 120, 483–494.
Schilling, T.F., Kimmel, C.B., 1997. Musculoskeletal patterning in the pharyngeal segments of the zebrafish embryo. Development 124, 2945–2960.
Schilling, T.F., Piotrowski, T., Grandel, H., Brand, M., Heisenberg, C.P., Jiang, Y.J., Beuchle, D., Hammerschmidt, M., Kane, D.A., Mullins, M.C., van Eeden, F.J., Kelsh, R.N., Furutani-Seiki, M., Granato, M., Haffter, P., Odenthal, J., Warga, R.M., Trowe, T., Nusslein-Volhard, C., 1996. Jaw and branchial arch mutants in zebrafish I: branchial arches. Development 123, 329–344.
Sharir, A., Stern, T., Rot, C., Shahar, R., Zelzer, E., 2011. Muscle force regulates bone shaping for optimal load-bearing capacity during embryogenesis. Development 138, 3247–3259.
Sperber, S.M., Dawid, I.B., 2008. Barx1 is necessary for ectomesenchyme proliferation and osteochondroprogenitor condensation in the zebrafish pharyngeal arches. Dev. Biol. 321, 101–110.
Thisse, C., Thisse, B., 2008. High-resolution in situ hybridization to whole-mount zebrafish embryos. Nat. Protoc. 3, 59–69.
Tissier-Seta, J.P., Mucchielli, M.L., Mark, M., Mattei, M.G., Goridis, C., Brunet, J.F., 1995. Barx1, a new mouse homeodomain transcription factor expressed in cranio-facial ectomesenchyme and the stomach. Mech. Dev. 51, 3–15.
Tremblay, P., Dietrich, S., Mericskay, M., Schubert, F.R., Li, Z., Paulin, D., 1998. A crucial role for Pax3 in the development of the hypaxial musculature and the long-range migration of muscle precursors. Dev. Biol. 203, 49–61.
Wada, N., Javidan, Y., Nelson, S., Carney, T.J., Kelsh, R.N., Schilling, T.F., 2005. Hedgehog signaling is required for cranial neural crest morphogenesis and chondrogenesis at the midline in the zebrafish skull. Development 132, 3977–3988.
Walker, C., Streisinger, G., 1983. Induction of mutations by gamma-rays in pregonial germ cells of zebrafish embryos. Genetics 103, 125–136.
Westerfield, M., 2000. The Zebrafish Book. University of Oregon Press, Eugene.
Westerfield, M., Liu, D.W., Kimmel, C.B., Walker, C., 1990. Pathfinding and synapse formation in a zebrafish mutant lacking functional acetylcholine receptors. Neuron 4, 867–874.
Yan, Y.L., Miller, C.T., Nissen, R.M., Singer, A., Liu, D., Kirn, A., Draper, B., Willoughby, J., Morcos, P.A., Amsterdam, A., Chung, B.C., Westerfield, M., Haffter, P., Hopkins, N., Kimmel, C., Postlethwait, J.H., 2002. A zebrafish sox9 gene required for cartilage morphogenesis. Development 129, 5065–5079.
Yan, Y.L., Willoughby, J., Liu, D., Crump, J.G., Wilson, C., Miller, C.T., Singer, A., Kimmel, C., Westerfield, M., Postlethwait, J.H., 2005. A pair of Sox: distinct and overlapping functions of zebrafish sox9 co-orthologs in craniofacial and pectoral fin development. Development 132, 1069–1083.
Yang, Y., Topol, L., Lee, H., Wu, J., 2003. Wnt5a and Wnt5b exhibit distinct activities in coordinating chondrocyte proliferation and differentiation. Development 130, 1003–1015.
Yelick, P.C., Schilling, T.F., 2002. Molecular dissection of craniofacial development using zebrafish. Crit. Rev. Oral Biol. Med. 13, 308–322.